Science of the Total Environment 955 (2024) 177063

Contents lists available at ScienceDirect

Science of the Total Environment

journal homepage: www.elsevier.com/locate/scitotenv

Calibration of Arctic ice core bromine enrichment records for past sea ice reconstructions

Federico Scoto [a,b,*], Niccolò Maffezzoli [b,c,a], Matthew B. Osman [d], Carlos A. Cuevas [e], Paul Vallelonga [f,g], Sumito Matoba [h], Yoshinori Iizuka [h], Alessandro Gagliardi [i,j], Cristiano Varin [b], François Burgay [k,b], Gianluca Pappaccogli [l], Joseph R. McConnell [m], Nathan Chellman [m], Carlo Barbante [a,b], Alfonso Saiz-Lopez [e], Andrea Spolaor [a]

[a] Institute of Polar Sciences, National Research Council, ISP-CNR, 30172 Venice, Italy
[b] Ca' Foscari University of Venice, Department of Environmental Sciences, Informatics and Statistics, Venice 30172, Italy
[c] Department of Earth System Science, University of California, Irvine, CA 92697, United States
[d] Department of Geography, University of Cambridge, Cambridge, UK
[e] Department of Atmospheric Chemistry and Climate, Institute of Physical Chemistry Blas Cabrera, CSIC, Madrid, Spain
[f] Physics of Ice Climate and Earth, Niels Bohr Institute, University of Copenhagen, Copenhagen N2200, Denmark
[g] UWA Oceans Institute, University of Western Australia, Crawley, WA 6009, Australia
[h] Institute of Low Temperature Science, Hokkaido University, Kita 19 Nishi 8, Kita-ku, Sapporo, Japan
[i] Department of Statistical Sciences, University of Padua, 35121 Padua, Italy
[j] Paleoclimate Dynamics Group, Alfred Wegener Institute, Helmholtz Centre for Polar and Marine Research, 27570 Bremerhaven, Germany
[k] Paul Scherrer Institute, Laboratory of Environmental Chemistry, 5232 Villigen, Switzerland
[l] Department of Environmental and Biological Sciences and Technologies, Univiversity of Salento, Lecce, Italy
[m] Desert Research Institute, Division of Hydrologic Sciences, 2215 Raggio Pkwy, Reno, NV 89512, USA

HIGHLIGHTS

- First statistical validation of bromine in ice cores as a sea ice proxy
- Br_{enr} values significantly correlate with first-year sea ice (FYSI) in Baffin Bay and Labrador Sea.
- Ice core Br_{enr} records overall captured historical Arctic sea ice variability.
- Complex regions need complementary proxies for long-term sea ice reconstructions.

GRAPHICAL ABSTRACT

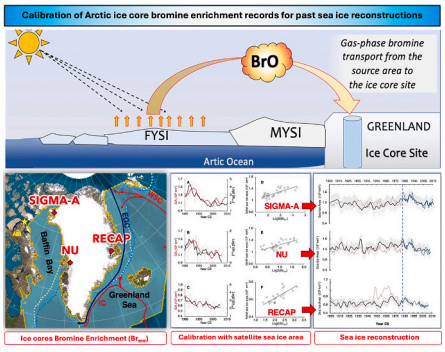

ARTICLE INFO

Editor: Christian Herrera

ABSTRACT

Bromine in ice cores has been proposed as a qualitative sea ice proxy to produce sea ice reconstructions for the polar regions. Here we report the first statistical validation of this proxy with satellite sea ice observations by combining bromine enrichment (with respect to seawater, Br_{enr}) records from three Greenlandic ice cores

* Corresponding author at: Institute of Polar Sciences, National Research Council, ISP-CNR, 30172 Venice, Italy.
E-mail address: federico.scoto@unive.it (F. Scoto).

https://doi.org/10.1016/j.scitotenv.2024.177063
Received 18 July 2024; Received in revised form 13 October 2024; Accepted 17 October 2024
Available online 22 October 2024

Keywords:
Arctic
Paleoclimate
Sea ice reconstructions
Proxy calibration
Bromine

(SIGMA-A, NU and RECAP) with satellite sea ice imagery, over three decades. We find that during the 1984–2016 satellite-era, ice core Br_{enr} values are significantly correlated with first-year sea ice formed in the Baffin Bay and Labrador Sea supporting that the gas-phase bromine enrichment processes, preferentially occurring over the sea ice surface, are the main driver for the Br_{enr} signal in ice cores. Moreover, in assessing Br_{enr}'s capability to record historical sea ice variability, we compare 20th-century Arctic Sea ice historical and proxy records with our reconstructions, based on an autoregressive–moving-average (ARMA) model, finding overall good agreement. While further enhancements are warranted, including site-specific calibrations and a comprehensive investigation into bromine transport-related concerns, this study presents a new method to quantitatively reconstruct past seasonal sea ice variability through bromine enrichment in ice cores.

1. Introduction

Over the past four decades, the Arctic has become a hotspot region of climate change with a warming trend nearly four times faster than the global average, a phenomenon commonly known as "Arctic amplification" (Rantanen et al., 2022). In response to atmospheric and oceanic temperature increase, Arctic sea ice has experienced a constant reduction of its summer extent (−12.7 % per decade relative to 1979–2021) (Meier et al., 2021), thickness (−2 m or −66 % between 1958 and 2018), and volume (-2.8×10^3 km^3 $decade^{-1}$ or −56 % compared to 1979–2023) (Schweiger et al., 2011). The observed ice thickness and volume reductions have been attributed to the loss of older and thicker sea ice present in the Arctic Ocean (Kacimi and Kwok, 2022; Kwok, 2018; Liu et al., 2020; Stroeve et al., 2007). Indeed, since 1980, the sea ice that survived at least one summer melting cycle, referred to as *multi-year sea ice* (MYSI), has declined by ~30 % and has been gradually replaced by thinner and younger *first-year sea ice* (FYSI), more prone to melting and wind-drifting than older ice (Kacimi and Kwok, 2022; Korosov et al., 2018; Kwok, 2018; Maslanik et al., 2011). The loss of MYSI is primarily due to the ice export from the Arctic Ocean through the Fram Strait (Smedsrud et al., 2017), however, it has also been observed that a significant fraction of MYSI disappears through melting within the Arctic basin (Ionita et al., 2016; Meier, 2017). If the rate of MYSI loss continues as in recent years, the Arctic Ocean is predicted to be seasonally ice-free before 2050 (Meier, 2017; Notz and SIMIP Community, 2020).

Due to its crucial impact on climate, ocean circulation, ecology and economics, Arctic Sea ice has been constantly monitored since the late 1970s through the extensive use of satellite observations and field measurements. In contrast, before the so-called *satellite era*, detailed sea ice reconstructions are sporadic and generally limited to the last two centuries, as provided by heterogeneous historical sources such as navigational charts, ship-based observations, and national ice services (Walsh et al., 2017).

To expand our knowledge both on pre-industrial sea ice variability at decadal-to-millennial time scale and to test the predictive skill of paleoclimate models, several geochemical markers from paleo-archives such as marine sediments and terrestrial ice cores have been used (Abram et al., 2013; Kinnard et al., 2011; Thomas et al., 2019; Vallelonga et al., 2021). The assemblage of microorganism and/or biomarkers in marine sediment typically provide longer records of sea ice although with some limitations mainly due to low temporal resolution (i.e. decadal to millennial time scales) and dating uncertainty (Thomas et al., 2019). Conversely, ice-core records, despite being provided at a high temporal resolution and in close relation with other climate and environmental forcing (e.g., temperature, greenhouse gas concentration, atmospheric circulation), can be mainly affected by post-depositional processes that need to be addressed for long-term reconstructions (Osman et al., 2017). The main sea ice proxies measured in polar ice cores include methanesulfonic acid (MSA), which indicates past sea ice extent and primary productivity, and sea salt sodium (ssNa), which provides information on sea ice cover and transport processes (Osman et al., 2019; Thomas et al., 2019). More recently, bromine - in particular, its enrichment factor over the Br/Na ratio in sea water (Br_{enr}), which appears to be stable in the snowpack after deposition at high accumulation sites (Spolaor et al., 2019) - has been explored in several studies as a potential tracer of past seasonal sea ice conditions (Spolaor et al., 2014, 2016a,b; Vallelonga et al., 2021; Scoto et al., 2022).

During polar springtime, solar radiation triggers a series of autocatalytic reactions involving ozone-depleting bromine species, sourced from the brine-enriched snow layer that deposits onto fresh sea-ice surfaces.

(Saiz-Lopez and Von Glasow, 2012; Simpson et al., 2015; Frey et al., 2020). Such bromine chemical cycles, referred to as "*bromine explosion*", lead to a marked enrichment of gas-phase reactive bromine species in the lower troposphere (Bougoudis et al., 2020; Saiz-Lopez and Von Glasow, 2012; Vallelonga et al., 2021). Following these explosion events, Br can undergo rapid oxidation with elemental mercury and dimethyl sulfide (leading to severe ozone loss in the polar boundary layer), heterogeneous recycling, and scavenging by atmospheric aerosols until being ultimately deposited as dry or wet deposition (Saiz-Lopez and Von Glasow, 2012; Simpson et al., 2015). As a net result, sea-ice related bromine emission processes increase the bromine-to-sodium ratio in springtime snowfall depositions over polar terrestrial glaciers, resulting in enriched bromine ($Br_{enr} > 1$) compared to deposition sourced purely from emission of bulk seawater aerosols (where $[Br]/[Na]_{seawater} = 0.0062$ and $Br_{enr} \approx 1$; Millero et al., 2008).

Based on this rationale, several Br_{enr} records from polar snow and ice core archives have been used to provide qualitative or semi-quantitative sea ice reconstructions at different time scales, both for the Arctic (Maffezzoli et al., 2019, 2021; Scoto et al., 2022; Sadatzki et al., 2020; Spolaor et al., 2016a,b; Vallelonga et al., 2021) and for Antarctica (Burgay et al., 2023; Spolaor et al., 2013; Vallelonga et al., 2017, 2021). So far, however, a robust statistical relation between absolute-ice core Br_{enr} and the extent of its potential sea ice-source area has never been provided.

In this study we perform a 30-y calibration of the Br_{enr} records from three Greenland ice cores (SIGMA-A, NU and RECAP) with satellite-derived regional sea ice variability in the Baffin Bay and Labrador Sea (BB), and in the Greenland Sea (GS), over the recent satellite period (1984 onwards). By correlating ice-core Br_{enr} levels with sea ice area variations in the identified bromine-source regions, we found a positive significant correlation thus providing, for the first time, a quantitative relationship between the two variables. We therefore applied to the recent Br_{enr} profiles of the selected ice cores, an autoregressive–moving-average (ARMA) model which returned respectively 111y (SIGMA-A), 108y (NU) and 107y (RECAP) records of regional sea ice changes. From a comparison with historical sea ice data, atmospheric reanalysis, and independents sea ice sensitive proxy records, our ice-core based reconstructions well captured the overall sub-regional sea ice variability, supporting the reliability of Br_{enr} as a tracer for long-term reconstructions of past regional sea ice changes.

2. Materials and methods

2.1. Ice cores

In spring 2017, the 60-m long "SIGMA-A" ice core, was drilled on the

Hayes Peninsula (78.05° N, 67.63° W, 1.490 m a.s.l.) (Fig. 1). The drilling site was located approximately 70 km north of the town of Qaanaaq, on a high accumulation area (0.27 m w. eq. y^{-1} between 1975 and 2010). The modern (1984–2016) SIGMA-A marine aerosols source region has been identified to be primarily the Baffin Bay (Kurosaki et al., 2020), which is nowadays covered only by seasonal sea ice (Fig. S1). The climatic information of SIGMA-A extends back to the last 110 years with a sub-seasonal time resolution for the whole record (Kurosaki et al., 2020; Matoba et al., 2018). The dating of the core was carried out by annual layer counting ($\delta^{18}O$, δD and other impurities measured at the University of Hokkaido) and the age uncertainty is estimated to be ±1 year for all samples (Kurosaki et al., 2020; Matoba et al., 2018).

In spring 2015, the 138-m long "NU" ice core was extracted from a high-elevation ice cap atop the Nuussuaq Peninsula, in west Greenland (70.49° N, 52.26° W, 2.010 m a.s.l.) (Osman et al., 2021) (Fig. 1). Model reconstructions show a marked temperature-driven increase in snow accumulation at the NU site over the last 200 years, passing from 0.26 to 0.36 m w. eq. y^{-1} (Osman et al., 2021). The ice core has been dated using 55 tie points obtained through chemical measurements of radiogenic ^{239}Pu, volcanic non-sea-salt sulfur, and anthropogenic Pb. The total record covers approximately the last 2 millennia (169 to 2015 CE). The present-day sea salt source region for the NU core is mainly centered on the lower Baffin Bay and the Labrador Seas, as inferred from a modern (1980–2013) atmospheric circulation reanalysis (Osman et al., 2021). The dynamics of the sea ice in these regions, governed by the variability of the Baffin Bay's southern sea ice edge position, is crucial for the formation of lighter sea water, which in turn influences the stratification and overall strength of the southern overturning circulation in the North Atlantic Ocean (Bi et al., 2019). The dating of the core in this depth range is carried out by annual layer counting ($\delta 18O$, δD and other impurities) and the age uncertainty is estimated to be ±1 year.

Finally, in spring 2015, the 584-m long "*Renland ice CAP*" (RECAP) ice core was retrieved on the Renland peninsula in coastal East Greenland (71.30 N, 26.72 W, 2315 m. a.s.l.) (Fig. 1). The annual accumulation rate at the coastal Renland site is much greater than that on the continental Greenland plateau with an average Holocene annual accumulation rate of ~0.41 w. eq. y^{-1} (Hansson, 1994; Hughes et al., 2020; Maffezzoli et al., 2021). The present-day RECAP core sampling region for marine aerosol has been identified to be the 50–85° N North Atlantic Ocean, as inferred from a modern (2000–2016) atmospheric circulation reanalysis (Corella et al., 2022; Cuevas et al., 2018; Maffezzoli et al., 2019). The ice core contains information on oceanic and sea ice-related processes mainly occurring in the Greenland Sea region (Corella et al., 2019; Cuevas et al., 2018; Maffezzoli et al., 2019, 2021). This region is dominated by a mixture of older sea ice exported out of the Arctic Ocean by the East Greenland current and locally formed seasonal sea ice which during winter extend from the older ice tongue eastwards to the North Atlantic Ocean (Tschudi et al., 2019) (Fig. S1). The dating in this depth range is carried out by annual layer counting and the age uncertainty is estimated to be ±1 year (Simonsen et al., 2019).

Given the high snow accumulation rate of the three sites considered in this study, we can assume a limited penetration of the ultraviolet (UV) radiation within the annual snowpack and a reduced or no capacity to promote photochemical reactions, especially in the UV-A (320–400 nm) and UV-B (290–320 nm) wavelength bands (Grannas et al., 2007). In turn, this suggests that the bromine records measured in the selected ice cores may not be significantly affected by post-depositional processes (Spolaor et al., 2019), at least on annual time scale (Maffezzoli et al.,

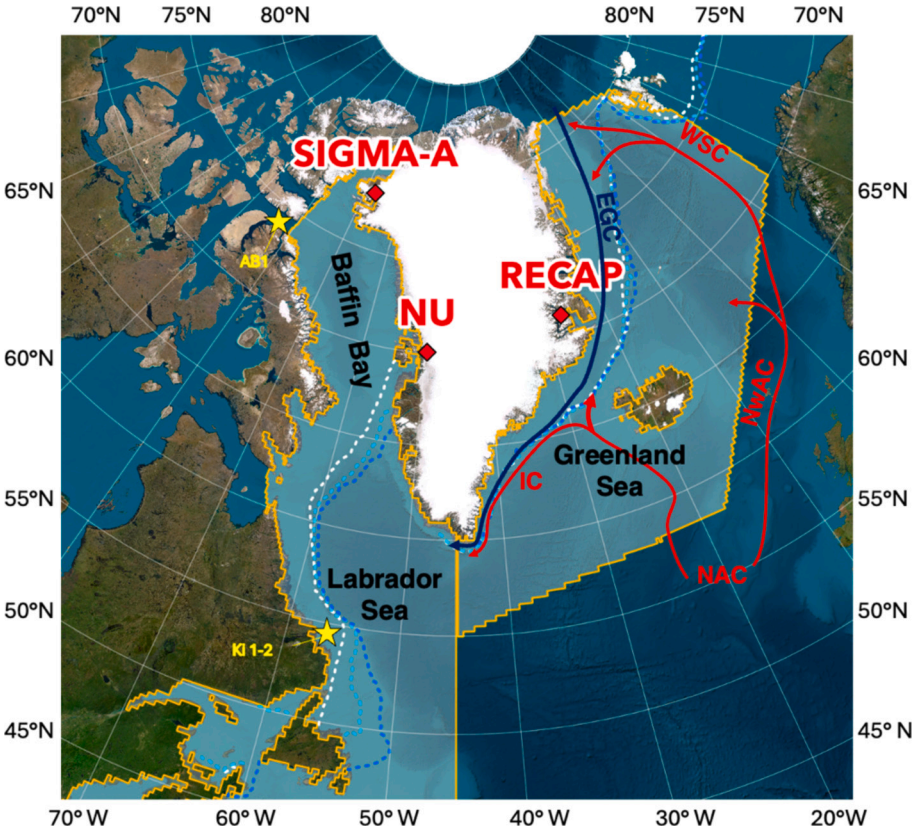

Fig. 1. Overview of the location sites of the ice cores used in this study. Ice core locations are marked by red squares. Yellow stars represent the location of the three algal samples from Halfar et al. (2013). The main warm and cold currents are indicated respectively with red and blue arrows: 'NAC': North Atlantic Current; 'NwAC': Norwegian Atlantic Current; 'WSC': West Spitsbergen Current; 'IC': Irminger Current; 'ECG': East Greenland Current. The shaded area contoured in orange are the NSIDC regional masks used to calculate historical Arctic sea ice concentration back to 1906 from Walsh et al. (2019) dataset. Dashed lines indicate the median sea ice extent between 1981 and 2010 in March (blue), April (light blue), and May (white) from NSIDC.

2021; Spolaor et al., 2014).

2.2. Ice cores analytical measurements and Br_{enr} factor

Meltwater discrete samples from the SIGMA-A ice core ($n = 564$), covering the 1906–2016 CE period, were analyzed at the CNR-ISP laboratories to detect bromine (Br) and sodium (Na) (Fig. S2-A). The first 240 samples, covering the satellite era (1979–2017 CE), were kept at their original resolution (~7 cm of ice integrating ~0.16 year/sample) and analyzed with an Inductively Coupled Plasma Sector Field Mass Spectrometry (ICP-SFMS; Element2, Thermo Fisher, Bremen, Germany) equipped with a cyclonic Peltier-cooled spray chamber (ESI, Omaha, US), following the methods described in earlier work (Spolaor et al., 2013). Analytical measurements on the remaining 324 samples, covering the pre-satellite era (1904–1978 CE; time-resolution of ~0.23 year/sample), were conducted with an Inductively Coupled Plasma Single Quadrupole Mass Spectrometry (ICP-SQMS, iCAP 168 RQ, Thermo Fisher Scientific, US) equipped with a collision cell reaction at the ISP-CNR laboratories.

The NU core was analyzed for a broad range of elements and chemical species using the continuous ice core analytical system at the Desert Research Institute (DRI) in Reno, NV, USA. Meltwater discrete samples ($n = 1550$), covering the 1906–2013 CE period, were analyzed for bromine and sodium concentrations by two High Resolution Inductively Coupled Mass Spectrometers operating in parallel (HR-ICP-MS, Thermo Element2, Bremen, Germany) at approximately 2 cm depth resolution. See Osman et al. (2021) for complete details on ice core dating and analysis.

Finally, meltwater discrete samples from the RECAP ice core ($n = 124$), covering the 1906–2012 CE period, were analyzed for bromine and sodium total concentrations by Collision Reaction Cell-Inductively Coupled Plasma-Mass Spectrometry (CRC-ICP-MS, Agilent 7500cx, Agilent, California, USA) at the CNR-ISP laboratories (Fig. S2-C). The analytical procedure is described in Maffezzoli et al. (2019).

For the three ice cores, annual mean Br and Na concentrations were calculated. Accordingly, Br_{enr} values were calculated as $Br_{enr} = (Br/Na)/(Br/Na)_{sea\ water}$, where (Br/Na) are the bromine and sodium concentrations in the ice samples and $(Br/Na)_{sea\ water} = 0.0062$ is the bromine-to-sodium mass ratio in seawater (Millero et al., 2008) (Fig. S2A–C).

2.3. Back-trajectories calculations

Air mass frequency plots were obtained from back trajectories computed using the HYSPLIT model (Hybrid Single-Particle Lagrangian Integrated Trajectory, Version 4 – January 2017) (Stein et al., 2015). For the three ice cores, the NCEP/NCAR Reanalysis data (Kalnay et al., 1996) from the National Weather Service's National Centers for Environmental Prediction provided by the NOAA's Air Resources Laboratory have been used. This reanalysis dataset has a 2.5° latitude × longitude spatial resolution, 17 levels from surface to 10 hPa and 6 h temporal resolution since 1/1/1948 to present. The 72 hour-long back trajectories arriving at SIGMA-A, NU, and RECAP ice core locations were started daily every 6 h (at 0:00, 6:00, 12:00 and 18:00 h) at 10 m above ground level for the periods 1984–2017 (SIGMA-A), 1984–2013 (NU), and 1984–2012 (RECAP), respectively. Only springtime (March, April, May) trajectories are considered, consistently with the timing of bromine recycling over sea ice. To ensure the exposure of air masses to marine sources of sea salt aerosols, only back trajectories spending at least 10 h in the marine boundary layer (>900 hPa or <1000 m a.s.l.) were considered, following the same methodology described in Maffezzoli et al. (2019).

2.4. Sea ice satellite data and potential bromine source area

2.4.1. Observation-based and historical sea ice data

The sea ice satellite product used to calibrate the recent Br_{enr} records of the three Greenland ice cores is the *Gridded Monthly Sea Ice Extent and Concentration, 1850 Onward, V.2* (Walsh et al., 2019). The dataset is based on an earlier product by Chapman and Walsh (1991; CW91) and combines modern Arctic Sea ice observations from satellite passive microwave data (Meier et al., 2013) with 16 historical sources, providing regional monthly sea ice concentration since 1850 (Walsh et al., 2017). The priority ordering procedure is the same of the CW91, along with analog and linear interpolation methods to spatially infill regions and times when observations are not available (Walsh et al., 2017, 2019). The dataset is released with each time-step corresponding to a single mid-month day and with a spatial resolution of 0.25° × 0.25°, covering the northern hemisphere north of 30°.

Prior to the period of satellite observations (1970s), however, the sea ice extent record holds large uncertainties due to the lack of direct and reliable observations in most parts of the Arctic. In particular, before 1953, sea ice reconstructions are constrained by direct observations almost only in summer months (i.e., when ships navigated Arctic waters) therefore the results obtained for this period are mainly generated by the infill strategy (Brennan et al., 2020). Acknowledging the limitations of the historical dataset before the satellite period, we compare our regional sea ice reconstructions based on SIGMA-A, NU, and RECAP Br_{enr} records with twentieth-century observation of the sea ice cover in the Baffin Bay and Labrador Sea sector and in the Greenland Sea.

2.4.2. Ice core's potential bromine source area (PBSA)

The first step to calibrate the Br_{enr} records is to identify the most-likely source regions of springtime bromine emissions. We refer to this sector as the potential bromine source area (PBSA) of a given ice core. To identify the PBSAs of the three ice cores, we combine both sea ice's presence and atmospheric transport by multiplying springtime (MAM) sea ice area (Fig. S3A) and air mass frequency maps sub-sampled at the same spatial resolution and calculated for the same period (Fig. S3B). The lowest pixel value displayed in the obtained bromine-source maps corresponds to an area covered by sea ice for just 1 month out of 3 (between March and May of each year) crossed only once by a back-trajectory directed to the ice core site (Fig. S3C). Reiterating this procedure for the satellite calibration period (1984 onward), averaging, and normalizing all the single-year bromine source maps obtained, we delimited the average springtime PBSA of SIGMA-A (1984–2016), NU (1984–2013), and RECAP (1984–2012), as shown in Fig. 2.

By applying this method to the selected ice cores, we noticed that the combined PBSA of the two ice cores from coastal western Greenland (i.e., SIGMA-A and NU), largely corresponds to the oceanic region extending from the higher Baffin Bay (BB) to the Labrador Seas (LS) (Fig. 2A). Therefore, for the purpose of Br_{enr} proxy calibration, we combined them into a more conservative area coinciding with the NSIDC regional sea ice mask of the Baffin Bay and Labrador Sea (Meier and Stewart, 2023) shown in Fig. 1.

For the RECAP ice core, the resulting PBSA includes three distinct sectors of the higher North Atlantic, which are namely the eastern Greenland Sea, part of central Baffin Bay and a portion of the Barents Sea (Fig. 2B). Although the total sea ice area, and in particular the seasonal sea ice area, in the eastern Greenland Sea sector is comparatively smaller with respect to the Baffin Bay and/or Barents Sea ones (Fig. S4A), due to its proximity to the RECAP ice core site, its contribution to the total PBSA accounts for 88 % while, the more distant Baffin Bay and the Barents Sea, only accounted respectively for 11 % and 1 % (Fig. S4B), consistent with also found in an earlier study by Maffezzoli et al. (2019). Given the relatively minor contribution of the latter two regions to the RECAP's PBSA, for the calibration of Br_{enr} proxy, we only considered sea ice variability limited to the Greenland Sea sector, (i.e. the East Greenland NSIDC regional mask; Meier and Stewart, 2023) shown in Fig. 1.

It's important to highlight the markedly different sea ice conditions that characterize the Baffin Bay and the Greenland Sea nowadays. In the former region, sea ice follows a well-paced seasonal cycle. Starting from

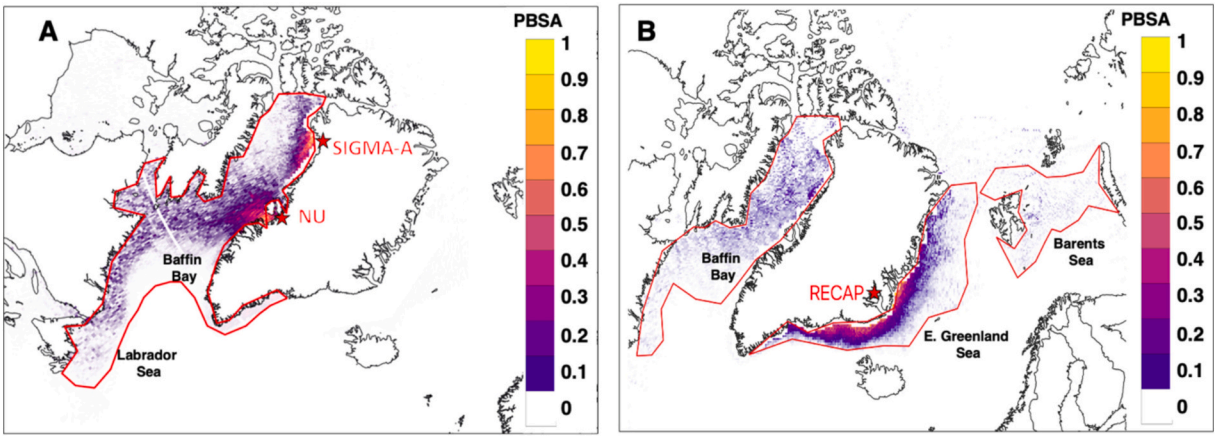

Fig. 2. The Potential Bromine Source Area (PBSA) of SIGMA-A, NU, and RECAP ice cores in the recent period (1984-onward). (A) The red contour delineates the combined PBSA of western Greenland ice cores (averaged and normalized for MAM 1984–2016 (SIGMA-A) and 1984–2013 (NU)). (B) Similarly, the RECAP's PBSA averaged and normalized over MAM 1984–2012. Among the three sectors identified, the East Greenland Sea accounts for most of the potential bromine contribution (~90 %), compared to Barents Sea and central Baffin Bay (~10 %).

the northwestern part, sea ice gradually forms in fall and extends southwestward to reach a complete sea ice cover of the Baffin Bay by March. In spring, usually in April, the sea ice gradually breaks in the North Water polynya (NOW) and along the western Greenland coast, moving westward until ice-free conditions occur in summer (August–September) (Gibb et al., 2015; Kurosaki et al., 2020; Mysak et al., 1996). In contrast, being mainly regulated by opposing oceanic currents, the colder and fresher East Greenland Current (EGC), and the warmer and saltier Irminger and North Atlantic Currents, (IC and NAC, respectively), sea ice conditions in the Greenland Sea are generally less predictable (Maffezzoli et al., 2021). In fact, the sea ice cover in this region is composed of a mixture of perennial and seasonal sea ice, with the former being pushed southwards across the Fram Strait by the EGC, and the latter forming in winter on its side and expanding southwards and eastwards until it encounters the western branches of the IC and NAC, which act as a physical constraint on the sea ice growth (Fig. 1) (Ionita et al., 2016).

3. Results and discussion

3.1. Correlation between recent sea ice variability and ice core's Br_{enr}

After identifying the oceanic regions potentially responsible for bromine deposition at the three ice core sites, we investigated whether a quantitative relationship exists between the recent sea ice variability and the Br_{enr} profiles recorded in the three Greenlandic ice cores (Fig. 3). To quantify the variations of the spring sea ice area within the PBSAs, we used recent (1984 onward) satellite observations from Walsh et al. (2019). Although satellite sea ice observations are available since 1979, we deliberately chose to start from 1984, as this corresponds to the starting date of sea ice age observations (Tschudi et al., 2019), which allowed us to distinguish between different sea ice types (*first-year* vs. *multi-year*) within the identified PBSAs.

We correlated the observed springtime (MAM) sea ice area of the Baffin Bay and Labrador Seas both with individual Br_{enr} records of SIGMA-A and NU cores (Fig. 3A–B), and with their compiled record obtained by averaging the individual Br_{enr} values for each year (Fig. 3C). Similarly, we correlated the observed spring sea ice area in the Greenland Sea with the RECAP's Br_{enr} record (Fig. 3D). To reduce any potential dating error, and to mitigate any artefacts of multi-year smoothing due to late 20th and 21st century surface meltwater percolation, we employ a 3-year moving average of annual Br_{enr} values while, to better represent the exponential nature of the inorganic bromine release from sea ice surfaces, we used base-2 logarithmic values of Br_{enr} (Spolaor et al., 2016a,b; Vallelonga et al., 2017). This transformation is also useful for the statistical analyses since it reduces the skewness of the observed values of Br_{enr} making them more adherent to the assumption of normality that is used thereafter for evaluation of the statistical significance of correlations.

For the Baffin Bay and Labrador Sea region, we found a positive significant correlation between the recent spring (MAM) sea ice area and log2(Br_{enr}), both for the individual records of the western Greenlandic ice cores records, with $r_{(SIGMA\_A)} = 0.63$ ($p < 0.001$), during 1984–2016 and $r_{(NU)} = 0.60$ ($p < 0.001$) during 1984–2013, and for their compiled one, with $r_{(SIGMA\_A+NU)} = 0.69$ ($p < 0.001$) during 1984–2013 (Fig. 3E–G; Table 1). Given the visual mismatch in the annual ice cores' Br_{enr} values and the sea ice area in the BB and LS (Fig. 3A–C), we also considered one-year lagged Br_{enr} variability, finding a remarkable increase of the correlations for SIGMA-A ($r_{(SIGMA\_A\text{-}1y)} = 0.69$, $p < 0.001$), NU ($r_{(NU\text{-}1y)} = 0.76$, $p < 0.001$), and, as expected, also for their compiled record ($r_{(SIGMA\_A\text{-}1y)+(NU\text{-}1y)} = 0.79$, $p < 0.001$) (Fig. 3I–M; Table 1). Consistent with ±1y age uncertainties in the depth–age constraints of the ice cores, we decided to consider SIGMA-A and NU's Br_{enr} series shifted by −1 year to reconstruct long-term regional sea ice variability.

Based on the fact that, during the recent period, the Baffin Bay and the Labrador Sea regions are characterized exclusively by seasonal sea ice (Tschudi et al., 2019) (Fig. S1), we can surmise that modern Br_{enr} profiles of SIGMA-A and NU cores are primarily modulated by changes of *first-year* sea ice (FYSI) rather than *multi-year* sea ice (MYSI), consistent with earlier observational studies (Bougoudis et al., 2020; Simpson et al., 2007). In this regard, we also examined a potential effect of the NOW polynya on atmospheric bromine deposition at SIGMA-A and NU ice core sites. Although a peak in the emission of organic bromine compounds from the ocean biosphere (i.e. CHBr3) is expected during summer and early autumn, their overall contribution to the total atmospheric bromine pool is relatively minor compared to the inorganic bromine compounds (i.e., Br_2 or BrO) released from heterogeneous bromine reactions over the sea ice surface during springtime bromine explosions (Bougoudis et al., 2020; Vallelonga et al., 2021). Long-term satellite observations of Arctic tropospheric BrO indeed show generally highest values in spring and lowest during summer and early autumn (Bougoudis et al., 2020), indicating inorganic sea ice-sourced bromine as a primary driver for modulating the Br_{enr} records in western Greenland ice cores during the recent period.

Finally, despite the concomitant presence of both FYSI and MYSI in the eastern Greenland Sea region during the satellite period (1984–2012; Fig. S1), we also found a positive significant correlation between spring sea ice area and RECAP's Br_{enr} ($r_{(RECAP)} = 0.73$, $p <$

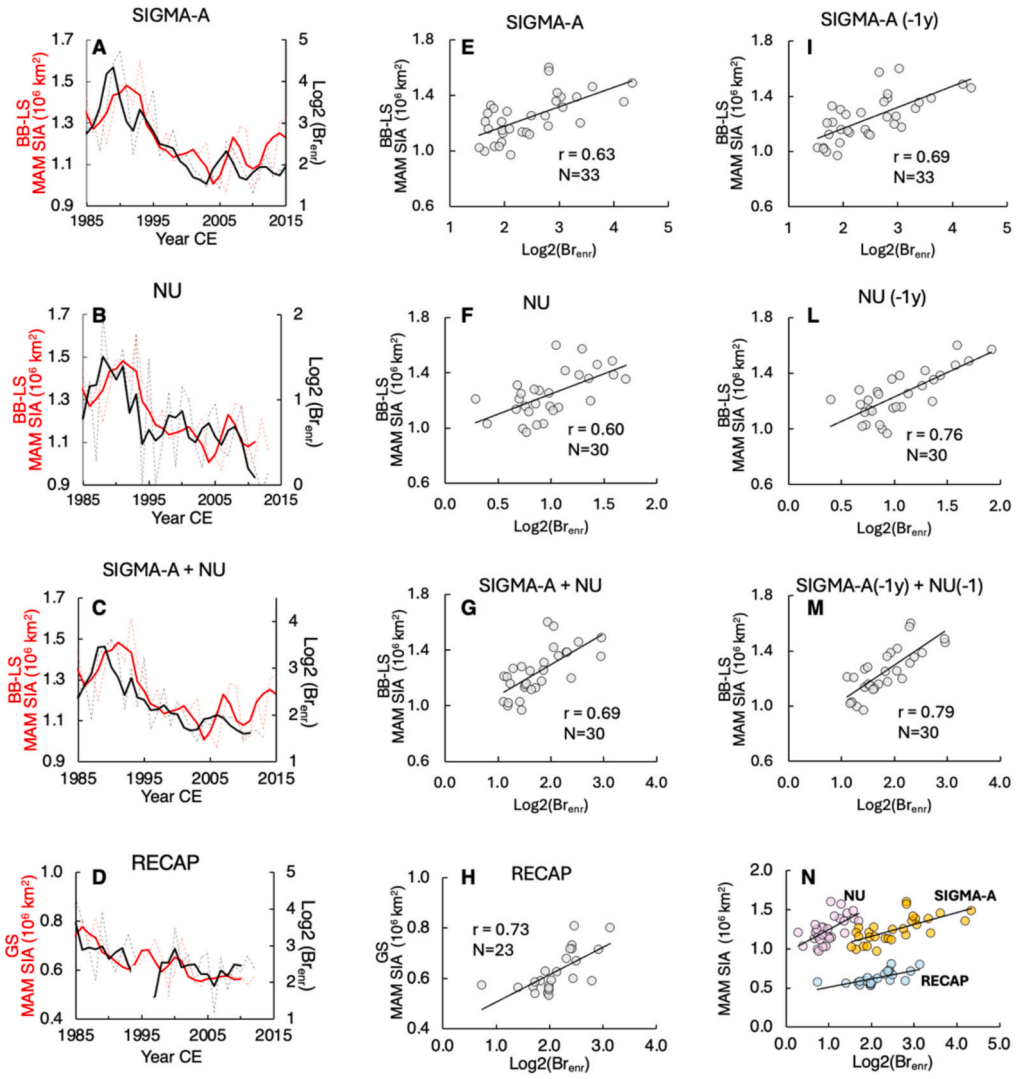

Fig. 3. Recent spring sea ice area (1984-onward) and Bromine enrichment records measured in the three Greenlandic ice cores. Red dashed curves in the panels A–D show the annual spring (MAM) sea ice area in the Baffin Bay and Labrador Sea sector (BB-LS) and in the Greenland Sea (GS) Black dashed curves indicate annual ice cores' bromine enrichment values from SIGMA-A (A), NU (B), their compiled record (C), and RECAP (D). Solid lines indicate 3y-moving averages. Panels E–H are the relative scatter plot showing the correlation between regional MAM sea ice area and Br_{enr} values (3-y moving average) from SIGMA-A (E), NU (F) their compiled record (G), and RECAP (H). Panels I–M show the same correlations of E-G but with the SIGMA-A and NU Br_{enr} series lagged of −1 year. Panel O summarizes panels E–G. All the scatter plots have a *p*-value < 0.001.

Table 1
Correlations between the Br_{enr} proxy (at lag 0 and −1 years) and satellite spring sea ice area in the relative ice cores' potential bromine source regions.

Ice core	PBSA	Period	Years	r	P-value
SIGMA-A	Baffin Bay and Labrador Sea	1984–2016	33	0.63	<0.001
NU	Baffin Bay and Labrador Sea	1984–2013	30	0.60	<0.001
Compiled (SIGMA-A + NU)	Baffin Bay and Labrador Sea	1984–2013	30	0.69	<0.001
SIGMA-A (−1y)	Baffin Bay and Labrador Sea	1983–2015	33	0.69	<0.001
NU (−1y)	Baffin Bay and Labrador Sea	1983–2012	30	0.76	<0.001
Compiled (SIGMA-A + NU) (−1y)	Baffin Bay and Labrador Sea	1983–2012	30	0.79	<0.001
RECAP	Greenland Sea	1984–2012	23	0.73	<0.001

0.001) (Fig. 3D and H; Table 1).

3.2. Regional sea ice reconstructions

Based on the significant correlation between log2(Br_{enr}) levels and the observed sea ice variability during the satellite era, we defined a site-specific predictive model of sea ice that, on the assumption of constant atmospheric transport/deposition processes over time, allows us to quantify past changes of seasonal sea ice within each ice core's PBSA. Given the high degree of year-to-year autocorrelation that exists in sea ice area time series, use of linear regression models that assume uncorrelated errors can lead to wrong conclusions. As such, we employed an autoregressive and moving average (ARMA) model that accounts for the potential serial correlation in the series. More specifically, we considered a linear regression of sea ice area on the log-transformed (Br_{enr}),

$$sea\_ice\_area(t) = \beta_0 + \beta_1 log_2 Br_{enr}(t) + \varepsilon(t),$$

where, β_0 and β_1 are the intercept and the slope of the regression line. To

take into account the potential serial autocorrelation, the error terms $\varepsilon(t)$ are assumed to follow the autoregressive and moving average model (Shumway and Stoffer, 2017),

$$\varepsilon(t) = \sum_{i=1}^{p} \varphi_i \varepsilon(t-i) + \eta(t) + \sum_{j=1}^{q} \theta_j \eta(t-j),$$

where $\eta(t)$ are white noise variables. The coefficients φ_i and θ_j are the parameters of the model, $i = 1, \ldots, p$ and $j = 1, \ldots, q$. The order of the model is given by p and q. We selected the model order using the Akaike Information Criterion (AIC; Shumway and Stoffer, 2007), with ARMA errors fitted using the regional sea ice area and the log-transformed Br_{enr} series for each site. As reported in Table 2, the best order for the models fitted to SIGMA-A and RECAP was $p = 0$ and $q = 1$, which corresponds to a moving average model of order 1; and $p = 0$ and $q = 0$ for NU and the compiled Br_{enr} record, which corresponds to standard regression model with uncorrelated errors (Table 2).

Finally, we tested the skill of the model employed by comparing our sea ice reconstructions obtained from the fitted statistical models with historical sea ice observational data from Walsh et al. (2019), along with atmospheric reanalysis and an independent proxy reconstruction from algal records (Halfar et al., 2013;Figs. 4–5).

3.2.1. *Baffin Bay and Labrador Sea ice evolution during the twentieth century*

Based on the individuals and compiled SIGMA-A and NU Br_{enr} records, we provide three distinct reconstructions of the spring seasonal sea ice variability in the Baffin Bay and Labrador Seas over the last century (1904–2016; Fig. 4A–C).

In general, the three reconstructions agree within the uncertainties with the springtime sea ice area reconstructed by Walsh et al. (2019). During the first decades of the twentieth century, both individual and compiled SIGMA-A and NU's Br_{enr} records show a multi-decadal variability accompanied by a gradual decline (more pronounced in SIGMA-A than in the NU core) until reaching their minimum on record, in late 1930s-early 1940s. The sea ice minimum indicated by the Br_{enr} proxy is consistent with the decrease in Baffin Bay sea ice concentration as also suggested in earlier studies by Cormier et al. (2016) and Kurosaki et al. (2020). During this period, indicated as the early twentieth century warming (ETCW), sea ice decreased in response to the strong surface warming in the Arctic (Bengtsson et al., 2004; Semenov and Latif, 2012), and to the concomitant warm phase of the Atlantic Multi-decadal Oscillation (AMO), given by the positive sea-surface temperature anomaly in the North Atlantic (Trenberth and Shea, 2006) (Fig. 4D–E). From 1940 to mid 1980s we observe a gradual increase of the spring sea ice cover consistent with the Arctic cooling between 1940 and 70 (Chylek et al., 2009) and the cold phase of the AMO that culminates with the most expanded sea ice conditions during the 1980–90s (Tang et al., 2004), also associated with a NAO-induced positive sea ice anomaly over the Labrador Sea region and eastern Canadian Subarctic (Grumet et al., 2001; Mysak et al., 1996; Strong and Magnusdottir, 2010) (Fig. 4D–F). After the spring sea ice maximum of mid-1990s, our proxy-based reconstructions well captured the recent declining trend observed by satellite measurements (Fetterer et al., 2017), occurring at an unprecedented rate since the end of ETCW.

Table 2
Estimates of the intercept β_0, the slope β_1 and the moving average coefficient θ_1 for the best autoregressive and moving average models according to AIC in the ice cores' potential bromine source regions. The moving average coefficient for NU is zero because AIC suggests to select a model with uncorrelated errors. Standard errors are reported within parentheses.

Site/Estimate	β_0	β_1	θ_1
SIGMA-A	0.88 (0.09)	0.15 (0.03)	0.33 (0.18)
NU	0.89 (0.06)	0.34 (0.05)	0.00 (–)
SIGMA-A + NU	0.78 (0.07)	0.26 (0.04)	0.00 (–)
RECAP	0.33 (0.07)	0.13 (0.03)	0.45 (0.18)

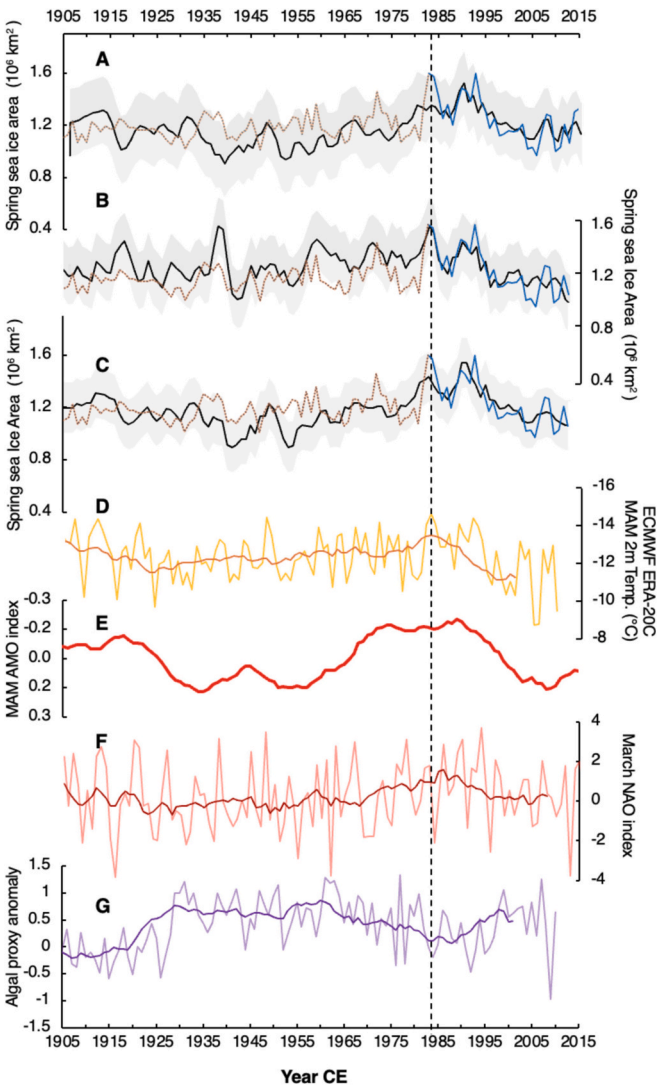

Fig. 4. Twentieth century sea ice reconstruction in the Baffin Bay and Labrador Sea. Black curves represent our reconstruction of the spring sea ice area based on Br_{enr} records from (A) SIGMA-A, (B) NU, and their compiled record (C). The statistical uncertainty is represented in gray with traditional 95 % prediction intervals. Solid blue lines represent the MAM sea ice area derived from satellite observations (1984-onward) while the dashed orange line is the reconstruction provided by Walsh et al. (2019). (D) Yellow curve represents 2 m air temperature from ECMWF-ERA20 reanalysis with 10-y moving average (orange). Values are averaged across 50-82 N and 80-45 W. (E) Red curve is the Atlantic Multi-decadal Oscillation (AMO) index (10-yr lowpass) based on Trenberth and Shea (2006), from CAS, NCAR. (F) March NAO index with a 10-y moving average (dark red) and (G) algal proxy record from Halfar et al. (2013) with 10-y moving average (violet). Lower values indicate more extended sea ice conditions.

The comparison of our reconstruction with historical sea ice data from Walsh et al. (2019) shows a noticeable agreement for the entire period for both SIGMA and NU, and especially for their compiled record (Fig. 4A–C). Most values from Walsh et al. (2019) historical reconstruction indeed fall within the 95 % prediction interval around our statistical reconstructions. Additionally, we also compare our reconstructions with an independent high-resolution proxy record from Halfar et al. (2013) which provides a reconstruction of the Baffin Bay sea ice variability over the last 646 years (Fig. 4G). This reconstruction is based on the growth and Mg/Ca ratio measured in long-lived calcified algae collected from three sites of the Canadian Arctic and Labrador Sea

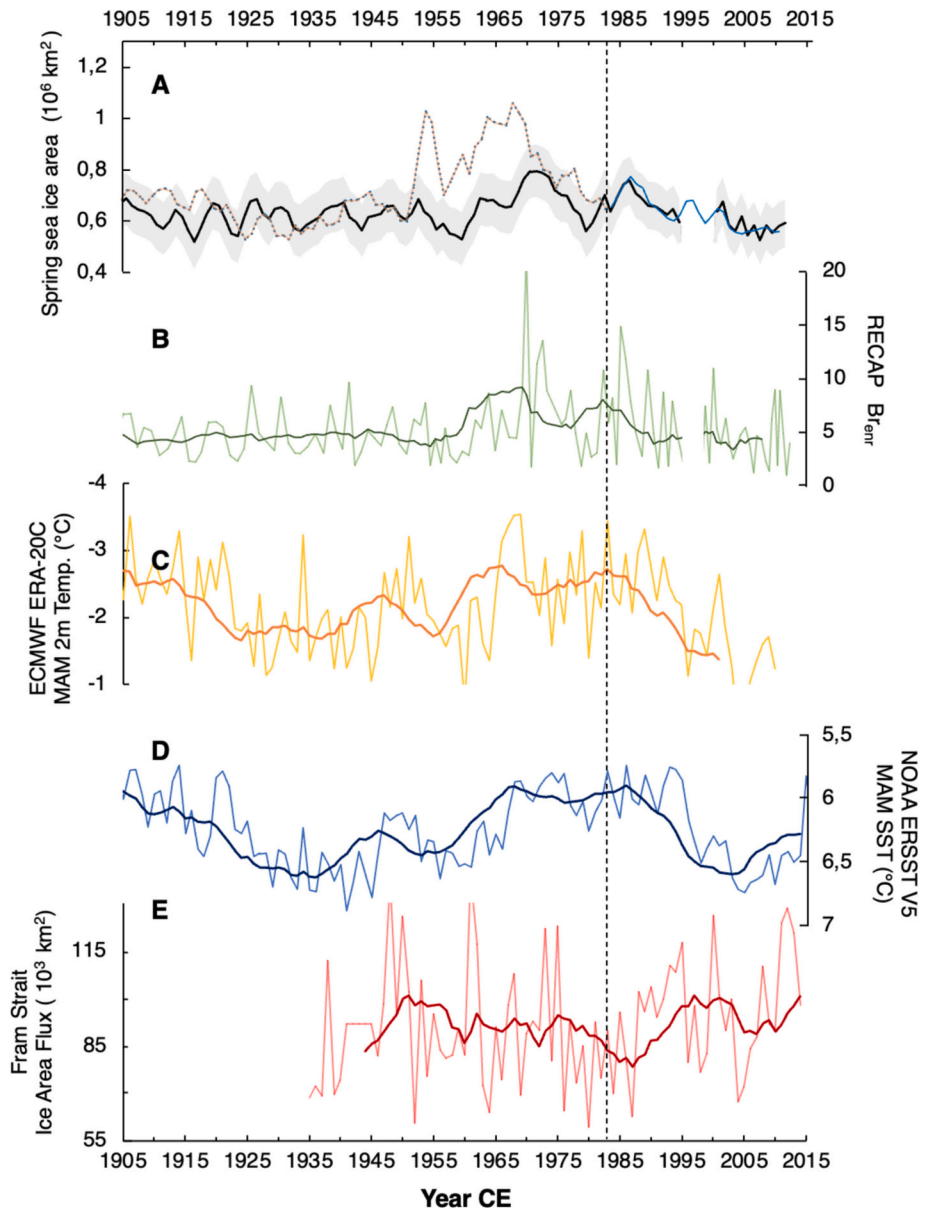

Fig. 5. Twentieth century sea ice reconstruction in the Greenland Sea. (A) Black curve represents our reconstruction of the spring sea ice area based on RECAP Br_{enr} record. The statistical uncertainty is represented in gray with traditional 95 % prediction intervals. Solid blue lines represent the MAM sea ice area derived from satellite observations (1984-onward) while the dashed orange line is the reconstruction provided by Walsh et al. (2019). (B) Green curve is the RECAP's pure Br_{enr} values plotted on normal scale. Empty space is due to missing data. (C) Yellow curve represents 2 m air temperature from ECMWF-ERA20 reanalysis with 10-y moving average (orange). Values are averaged across 80-60 N; 15E-45 W (D) Light blue curve represents MAM sea surface temperature from NOAA ERSST V.5 reanalysis with 10-y moving average (dark blue) averaged across 80–60 N; 15E–45 W. (E) Fram Strait spring sea ice export variability extracted from Smedsrud et al. (2017) with 10y-y moving average (red).

representing summer sea ice abundance (Halfar et al., 2013) (Fig. 1). Among the sea ice reconstructions based on individuals SIGMA-A and NU Br_{enr} records, the former is largely consistent with the sea ice anomaly inferred from the algal proxy record, with an anti-correlation of 15-yr low-pass filtered annual data equal to $r = -0.59$, during 1912–2003 (note that algal sea ice record is inversely correlated with sea ice area), which increases to $r = -0.88$ during 1926–2003. In contrast, the correlation with the reconstruction based on individual NU's Br_{enr} record is not significant for the entire period ($r = -0.01$) but become noticeable only during the recent period 1980–2010 ($r = -0.63$). We explain the relative discrepancy between NU's Br_{enr} and the algal record observed before the satellite period as the result of different sea surface conditions in the Labrador Sea and Baffin Bay regions which may have eventually affected the local sea ice variability between the higher and lower Baffin Bay as also suggested in an earlier study (Gibb et al., 2015). This in turn is reflected also on the correlation between the algal record and the compiled Br_{enr} record over 1906–2010, that is still significant ($r = -0.43$) but lower than the correlation found for SIGMA-A only.

Finally, assuming predominant seasonal ice conditions in Baffin Bay (Kurosaki et al., 2020) and limited sea ice inflow from the Canadian Arctic (Bi et al., 2019), we estimated the expected amount of newly formed ice each year ($FYSI_{EXP}$), based on monthly sea ice data from Walsh et al. (2019). This quantity is obtained by subtracting the previous sea ice minimum, generally reached in September, from the next sea ice maximum, generally occurring in March. The $FYSI_{EXP}$ calculated for the last century, varies between 79 and 98 % of the total Baffin Bay sea ice cover, suggesting seasonal ice as the predominant sea ice regime over the last century. This result provides an additional indication that ice

cores' Br_{enr} is reasonably able of capturing first-year sea ice changes, therefore, we point out the Baffin Bay and Labrador Sea basins as a suitable oceanic region for further ice core's Br_{enr} -based sea ice reconstructions.

3.2.2. Greenland Sea ice evolution during the twentieth century

Analogously to SIGMA-A and NU, we employ the RECAP's Br_{enr} record to reconstruct the spring sea ice area in the Greenland Sea during the period 1906–2012 (Fig. 5A). In general, except for a limited period between 1950 and 1970, our proxy-based sea ice reconstruction is consistent, within the uncertainties of the ARMA model, with the total springtime Greenland Sea sea-ice area reconstructed by Walsh et al. (2019), especially during the recent declining trend observed between 1984 and 2012 ($r_{obs\text{-}rec} = 0.66$, $P < 0.001$).

From the beginning of the twentieth century until late 1950s, our proxy record indicates a decadal variability of the spring sea ice cover in the Greenland Sea, without suggesting, however, any high-amplitude sea ice variation (Figs. 5B; S2C). This differs from the historical dataset which indicate local minima sea ice conditions around 1925 and 1935 (Fig. 5A). Interestingly, historical data of spring sea ice area in the Greenland Sea region, show a marked increase during 1950–1970, with a positive anomaly of the total sea ice area reaching its maximum on record, (+46 % compared to 1906–2012) between 1968 and 70 (Walsh et al., 2019; Figs. 5A and S5A–B). Concurrently, also the RECAP's Br_{enr} record shows a local maximum with a positive Br_{enr} anomaly of +45 % observed during the same period (Figs. 5B; S2C). The extended spring sea ice condition suggested by our proxy is also consistent with the lower atmospheric and sea surface temperatures (Fig. 5C–D), thus also with a cold phase of the AMO (Fig. 4E), and with the rapid drop in near-surface salinity observed in the northern North Atlantic in late 1960s and early 70s, commonly referred to as the Great Salinity Anomaly (GSA). Such sea ice anomaly originated in the Arctic Ocean but, after summer melting, propagated to west Greenland as a salinity/temperature anomaly in 1–2 years (Belkin et al., 1998; Dickson et al., 1988; Häkkinen, 1993; Hodson et al., 2014; Ionita et al., 2016; Schmith and Hansen, 2003).

The connection between a more extended sea ice area and higher Br_{enr} values, however, is not always straightforward. Before the sharp increase in the late 1960s, in fact, we noticed an opposite trend between the Greenland Sea sea ice area and the RECAP's $Br_{enr.}$, with the former relatively higher than the long-term average ($GS_{anom.} = +47$ % between 1953 and 55), and the latter lower than average ($Br_{enr\text{-}anom.} = -4$ %) during the same years.

We explain this condition with an increase in the MYSI portion in the Greenland Sea. Based on previous studies referring to glacial-interglacial transitions, in fact, is likely that portions of MYSI developed along the East Greenland coast during glacial periods, leading to an eastward displacement of the FYSI edge from the coast (Maffezzoli et al., 2021). For ice core sites like RECAP, located ~200 km inland, such displacement could have been caused a decrease of the Br_{enr} signal due to the increased distance of the bromine gas phase source from the ice core site (Vallelonga et al., 2021). As a modern analog, the relatively low RECAP's Br_{enr} observed in mid-1950s, can be explained with a period of enhanced MYSI export across the Fram Strait as also supported by the reconstructed Fram Strait ice volume flux that shows a positive anomaly of +20 % compared to 1935–2014 period in the same years (Schmith and Hansen, 2003; Smedsrud et al., 2017) (Fig. 5E).

After reaching its largest extent on record, in spring 1969 (S5B), total Arctic sea ice coverage has undergone a protracted decline until its minimum on record observed in 2012 (S5C) and still undergoing to the present day (Brennan et al., 2020; Kwok, 2018). Since the late 1970s, satellites have observed a constant decrease of the springtime sea ice area also in the Greenland Sea (-0.77×10^5 km^2/decade or −51 % in four decades). In particular, based on sea ice age data (Tschudi et al., 2019) the FYSI component in the Greenland Sea have overall declined in line with the total sea ice trend ($r = 0.83$, $p < 0.001$). Conversely, the MYSI component gradually increased from ~25 % in 1984 to ~40 % in 2012, consistent with the enhanced sea ice export linked to the inter-annual variability of the Beaufort Gyre and increased surface pressure over Greenland (Rigor et al., 2002; Smedsrud et al., 2011, 2017; Wei et al., 2019; Yang et al., 2023).

Our previous findings indicate that ice core's Br_{enr} is effectively able to capture sea ice changes during the satellite period when the sea ice regime is primarily seasonal. However, in conditions where both FYSI and MYSI are present, (i.e. in the Greenland Sea), our proxy calibration is reliable only when the FYSI/MYSI ratio is within the range observed during the satellite-calibration period (i.e. 1984–2012). This limitation may explain the discrepancy between our reconstruction and Walsh et al. data during the mid-1950s, when -likely due to an increased proportion of MYSI in the Greenland Sea- the FYSI/MYSI ratio became considerable different from the recent one. In addition, another aspect that must be considered is the different peak season in snow accumulation between western and eastern Greenland. In West Greenland, maximum snow accumulation usually occurs in spring/summer (April to July), thus it is very likely that the deposited snow may have recorded the atmospheric imprint of the seasonal bromine explosions occurring on the sea ice surface. In contrast, in Eastern Greenland, snow accumulation is influenced by Atlantic storms bringing heavy snowfall mainly during the winter season (November to March) (Cappelen, 2020), so with a limited potential of capturing the inorganic bromine compounds released during the polar spring. For this reason, we suggest treating bromine enrichment records from eastern Greenland ice cores more cautiously for long-term reconstructions of total sea-ice variability, as the presence of MYSI and/or a different snow accumulation season could weaken (or even nullify) the relationship found instead for western Greenland ice cores.

4. Conclusions

Through the calibration of Br_{enr} records from three Greenland ice cores with satellite (post-1984) sea ice variability in their relative potential bromine source areas (i.e. the potential sea ice area exposed to the mean surface wind field directed to the ice core site), we provided for the first time a quantitative relationship, supporting the reliability of the ice core proxy for regional Arctic sea ice reconstructions. Furthermore, using linear regression of satellite sea ice data on modern $\log2(Br_{enr})$ records with autoregressive and moving average errors, we obtained a reasonable reconstruction of the overall sea ice variability during the last century in two distinct Arctic sub-regions, namely the Baffin Bay/Labrador Sea and the Greenland Sea.

The agreement between the proxy-based reconstructions and the observed Baffin Bay and Labrador Sea total sea ice area is strongest during the satellite era, from 1984 - onward, and weakest prior to this period, despite we acknowledge the larger uncertainties of the reference dataset especially before 1953.

The comparison between our sea ice reconstructions and an independent algal proxy record, shows a remarkably good agreement over the last century for the SIGMA-A core, and an overall good agreement during the recent period for both SIGMA-A and NU ice cores. Similarly, the Br_{enr} record of the RECAP ice core was calibrated with the recent observed sea ice changes in the Greenland Sea, identified as the main ice core's potential bromine source area. We hence provide a reconstruction of the Greenland Sea sea ice variability during the twentieth century. We obtain an overall good agreement with the historical data used for comparison, excluding a delimited period characterized by cold temperatures and enhanced sea ice export from the Fram Strait gateway (i.e. suggesting enhanced MYSI conditions in the Greenland Sea).

Finally, based on the linear relationship found between the compiled Br_{enr} record in coastal western Greenlandic ice cores and the recent seasonal or *first-year* sea ice variability in the Baffin Bay and Labrador Sea, we recommend this particular oceanic region as an ideal site for future Br_{enr}-based sea ice reconstructions. In contrast, the interplay

between *first-year* and *multi-year* sea ice, together with a more wintry snow accumulation period in eastern Greenland ice cores, can significantly affect the Br_{enr} proxy sensitiveness to sea ice changes, making long-term sea ice reconstruction for the Greenland Sea region more complex. This in turn calls the need for complementary proxy records, especially from the oceanic compartment (i.e. marine sediments), to be employed in addition to Br_{enr} for a more comprehensive overview of past sea ice export/variability.

As further testing and site-specific calibrations are expected for other Arctic high snow accumulation ice core sites -and issues related to marine aerosol transport need to be further investigated by the ice core community- the results obtained in this study highlight the advancements of Br_{enr} as a reliable proxy for past sea ice reconstructions, especially for oceanic regions with predominant seasonal sea ice conditions.

CRediT authorship contribution statement

Federico Scoto: Writing – review & editing, Writing – original draft, Visualization, Validation, Methodology, Investigation, Formal analysis, Data curation, Conceptualization. **Niccolò Maffezzoli:** Writing – review & editing, Visualization, Investigation, Formal analysis, Data curation. **Matthew B. Osman:** Writing – review & editing, Investigation, Formal analysis, Data curation. **Carlos A. Cuevas:** Writing – review & editing, Investigation, Formal analysis, Data curation. **Paul Vallelonga:** Writing – review & editing, Formal analysis, Data curation. **Sumito Matoba:** Writing – review & editing, Resources, Investigation, Funding acquisition, Formal analysis. **Yoshinori Iizuka:** Writing – review & editing, Resources, Funding acquisition, Formal analysis. **Alessandro Gagliardi:** Writing – review & editing, Methodology, Investigation, Formal analysis, Data curation. **Cristiano Varin:** Writing – review & editing, Methodology, Investigation, Formal analysis, Data curation. **François Burgay:** Writing – review & editing, Investigation, Formal analysis. **Gianluca Pappaccogli:** Writing – review & editing, Visualization, Formal analysis, Data curation. **Joseph R. McConnell:** Writing – review & editing, Investigation, Formal analysis. **Nathan Chellman:** Writing – review & editing, Investigation, Formal analysis. **Carlo Barbante:** Writing – review & editing, Supervision, Investigation, Formal analysis. **Alfonso Saiz-Lopez:** Writing – review & editing, Supervision, Investigation, Formal analysis, Conceptualization. **Andrea Spolaor:** Writing – review & editing, Supervision, Investigation, Funding acquisition, Formal analysis, Conceptualization.

Declaration of competing interest

The authors declare that they have no known competing financial interests or personal relationships that could have appeared to influence the work reported in this paper.

Acknowledgments

The SIGMA-A ice core processing and transportation was partly supported by Japan Society for the Promotion of Science (JSPS) KAKENHI Grant Numbers JP18H05292, and the Arctic Challenge for Sustainability II Program (ArCS II: JPMXD1420318865). Funding for retrieval and analysis of the NU ice core was provided by the US National Science Foundation (NSF) Arctic System Science Program award OPP-1205196 and ARC-1205062. Geospatial support for this work was provided by the Polar Geospatial Center under NSF-OPP awards 1043681 and 1559691. The RECAP ice coring effort was financed by the Danish Research Council through a Sapere Aude grant, the NSF through the Division of Polar Programs, the Alfred Wegener Institute Helmholtz Centre for Polar and Marine Research, and the European Research Council under the European Community's Seventh Framework Programme (FP7/2007-2013)/ERC grant agreement 610055 through the Ice2Ice project and the Early Human Impact project (267696). This project has received funding from the European Union's Horizon 2020 research and innovation programme under grant agreement no. 689443 via project iCUPE (Integrative and Comprehensive Understanding on Polar Environments).

Appendix A. Supplementary data

Supplementary data to this article can be found online at https://doi.org/10.1016/j.scitotenv.2024.177063.

Data availability

Data will be made available on request.

References

Abram, N.J., Wolff, E.W., Curran, M.A.J., 2013. A review of sea ice proxy information from polar ice cores. Quat. Sci. Rev. https://doi.org/10.1016/j.quascirev.2013.01.011.

Belkin, I.M., Levitus, S., Antonov, J., Malmberg, S.A., 1998. "Great salinity anomalies" in the North Atlantic. Prog. Oceanogr. https://doi.org/10.1016/S0079-6611(98)00015-9.

Bengtsson, L., Semenov, V.A., Johannessen, O.M., 2004. The early twentieth-century warming in the arctic - a possible mechanism. J. Climate 17 (20), 4045–4057. https://doi.org/10.1175/1520-0442(2004)017<4045:TETWIT>2.0.CO;2.

Bi, H., Zhang, Z., Wang, Y., Xu, X., Liang, Y., Huang, J., Liu, Y., Fu, M., 2019. Baffin Bay sea ice inflow and outflow: 1978–1979 to 2016–2017. Cryosphere 13 (3), 1025–1042. https://doi.org/10.5194/tc-13-1025-2019.

Bougoudis, I., Blechschmidt, A.-M., Richter, A., Seo, S., Burrows, J.P., Theys, N., Rinke, A., 2020. Long-term time series of Arctic tropospheric BrO derived from UV–VIS satellite remote sensing and its relation to first-year sea ice. Atmospheric Chemistry and Physics 20 (20), 11869–11892. https://doi.org/10.5194/acp-20-11869-2020.

Brennan, M.K., Hakim, G.J., Blanchard-Wrigglesworth, E., 2020. Arctic sea-ice variability during the instrumental era. Geophys. Res. Lett. 47 (7). https://doi.org/10.1029/2019GL086843.

Burgay, F., Fernández, R.P., Segato, D., Turetta, C., Blaszczak-Boxe, C.S., Rhodes, R.H., Scarchilli, C., Ciardini, V., Barbante, C., Saiz-Lopez, A., Spolaor, A., 2023. 200-Year ice core bromine reconstruction at Dome C (Antarctica): observational and modelling results. Cryosphere 17 (1), 391–405. https://doi.org/10.5194/tc-17-391-2023.

Cappelen, J., 2020. Greenland - DMI historical climate data collection 1784-2019. In: DMI-Report, 20–04.

Chapman, W.L., Walsh, J.E., 1991. Long-range prediction of regional sea ice anomalies in the Arctic. Weather Forecast. 6 (2). https://doi.org/10.1175/1520-0434(1991)006<0271:lrpors>2.0.co;2.

Chylek, P., Folland, C.K., Lesins, G., Dubey, M.K., Wang, M., 2009. Arctic air temperature change amplification and the Atlantic Multidecadal Oscillation. Geophys. Res. Lett. 36 (14). https://doi.org/10.1029/2009GL038777.

Corella, J.P., Maffezzoli, N., Alberto Cuevas, C., Vallelonga, P., Spolaor, A., Cozzi, G., Müller, J., Vinther, B., Barbante, C., Astrid Kjær, H., Edwards, R., Saiz-Lopez, A., 2019. Holocene atmospheric iodine evolution over the North Atlantic. Climate of the Past 15 (6), 2019–2030. https://doi.org/10.5194/cp-15-2019-2019.

Corella, J.P., Maffezzoli, N., Spolaor, A., Vallelonga, P., Cuevas, C.A., Scoto, F., Müller, J., Vinther, B., Kjær, H.A., Cozzi, G., Edwards, R., Barbante, C., Saiz-Lopez, A., 2022. Climate changes modulated the history of Arctic iodine during the Last Glacial Cycle. Nature Communications 13 (1). https://doi.org/10.1038/s41467-021-27642-5.

Cormier, M.A., Rochon, A., de Vernal, A., Gélinas, Y., 2016. Multi-proxy study of primary production and paleoceanographical conditions in northern Baffin Bay during the last centuries. Mar. Micropaleontol. 127. https://doi.org/10.1016/j.marmicro.2016.07.001.

Cuevas, C.A., Maffezzoli, N., Corella, J.P., Spolaor, A., Vallelonga, P., Kjær, H.A., Simonsen, M., Winstrup, M., Vinther, B., Horvat, C., Fernandez, R.P., Kinnison, D., Lamarque, J.F., Barbante, C., Saiz-Lopez, A., 2018. Rapid increase in atmospheric iodine levels in the North Atlantic since the mid-20th century. Nat. Commun. 9 (1), 1–6. https://doi.org/10.1038/s41467-018-03756-1.

Dickson, R.R., Meincke, J., Malmberg, S.-A., Lee, A.J., 1988. The "great salinity anomaly" in the Northern North Atlantic 1968–1982. Prog. Oceanogr. 20 (2), 103–151. https://doi.org/10.1016/0079-6611(88)90049-3.

Fetterer, F., Knowles, K., Meier, W.N., Savoie, M., Windnagel, A.K., 2017. Sea Ice Index, Version 3 [Data Set]. National Snow and Ice Data Center, Boulder, Colorado USA (Date Accessed 05-20-2024).

Frey, M.M., Norris, S.J., Brooks, I.M., Anderson, P.S., Nishimura, K., Yang, X., Jones, A.E., Nerentorp Mastromonaco, M.G., Jones, D.H., Wolff, E.W., 2020. First direct observation of sea salt aerosol production from blowing snow above sea ice. Atmos. Chem. Phys. 20, 2549e2578.

Gibb, O.T., Steinhauer, S., Fréchette, B., de Vernal, A., Hillaire-Marcel, C., 2015. Diachronous evolution of sea surface conditions in the labrador sea and baffin bay since the last deglaciation. Holocene 25 (12). https://doi.org/10.1177/0959683615591352.

Grannas, A.M., Jones, A.E., Dibb, J., Ammann, M., Anastasio, C., Beine, H.J., Bergin, M., Bottenheim, J., Boxe, C.S., Carver, G., Chen, G., Crawford, J.H., Dominé, F., Frey, M. M., Guzmán, M.I., Heard, D.E., Helmig, D., Hoffmann, M.R., Honrath, R.E., et al., 2007. An overview of snow photochemistry: evidence, mechanisms and impacts. Atmospheric Chemistry and Physics 7 (16), 4329–4373. https://doi.org/10.5194/acp-7-4329-2007.

Grumet, N.S., Wake, C.P., Mayewski, P.A., Zielinski, G.A., Whitlow, S.I., Koerner, R.M., Fisher, D.A., Woollett, J.M., 2001. Variability of sea-ice extent in Baffin Bay over the last millennium. Clim. Change 49 (1–2), 129–145. https://doi.org/10.1023/A:1010794528219.

Häkkinen, S., 1993. An Arctic source for the great salinity anomaly: a simulation of the Arctic ice-ocean system for 1955–1975. J. Geophys. Res. Oceans 98 (C9), 16397–16410. https://doi.org/10.1029/93JC01504.

Halfar, J., Adey, W.H., Kronz, A., Hetzinger, S., Edinger, E., Fitzhugh, W.W., 2013. Arctic sea-ice decline archived by multicentury annual-resolution record from crustose coralline algal proxy. Proceedings of the National Academy of Sciences of the United States of America 110 (49). https://doi.org/10.1073/pnas.1313775110.

Hansson, M.E., 1994. The Renland ice core. A Northern Hemisphere record of aerosol composition over 120,000 years. Tellus B 46 (5). https://doi.org/10.1034/j.1600-0889.1994.t01-4-00005.x.

Hodson, D.L.R., Robson, J.I., Sutton, R.T., 2014. An anatomy of the cooling of the North Atlantic Ocean in the 1960s and 1970s. J. Climate 27 (21), 8229–8243. https://doi.org/10.1175/JCLI-D-14-00301.1.

Hughes, A.G., Jones, T.R., Vinther, B.M., Gkinis, V., Max Stevens, C., Morris, V., Vaughn, B.H., Holme, C., Markle, B.R., White, J.W.C., 2020. High-frequency climate variability in the Holocene from a coastal-dome ice core in east-central Greenland. Climate of the Past 16 (4). https://doi.org/10.5194/cp-16-1369-2020.

Ionita, M., Scholz, P., Lohmann, G., Dima, M., Prange, M., 2016. Linkages between atmospheric blocking, sea ice export through Fram Strait and the Atlantic Meridional Overturning Circulation. Sci. Rep. 6 (1), 32881. https://doi.org/10.1038/srep32881.

Kacimi, S., Kwok, R., 2022. Arctic Snow Depth, Ice Thickness, and Volume From ICESat-2 and CryoSat-2: 2018–2021. https://doi.org/10.1029/2021GL097448 (2018–2021).

Kalnay, E., Kanamitsu, M., Kistler, R., Collins, W., Deaven, D., Gandin, L., Iredell, M., Saha, S., White, G., Woollen, J., Zhu, Y., Chelliah, M., Ebisuzaki, W., Higgins, W., Janowiak, J., Mo, K.C., Ropelewski, C., Wang, J., Leetmaa, A., et al., 1996. The NCEP/NCAR 40-year reanalysis project. Bull. Am. Meteorol. Soc. 77 (3), 437–472. https://doi.org/10.1175/1520-0477(1996)077<0437:TNYRP>2.0.CO;2.

Kinnard, C., Zdanowicz, C.M., Fisher, D.A., Isaksson, E., De Vernal, A., Thompson, L.G., 2011. Reconstructed changes in Arctic sea ice over the past 1,450 years. Nature 479 (7374), 509–512. https://doi.org/10.1038/nature10581.

Korosov, A., Rampal, P., Toudal Pedersen, L., Saldo, R., Ye, Y., Heygster, G., Lavergne, T., Aaboe, S., Girard-Ardhuin, F., 2018. A new tracking algorithm for sea ice age distribution estimation. Cryosphere 12 (6), 2073–2085. https://doi.org/10.5194/tc-12-2073-2018.

Kurosaki, Y., Matoba, S., Iizuka, Y., Niwano, M., Tanikawa, T., Ando, T., Hori, A., Miyamoto, A., Fujita, S., Aoki, T., 2020. Reconstruction of sea ice concentration in northern Baffin Bay using deuterium excess in a coastal ice core from the northwestern Greenland Ice Sheet. J. Geophys. Res. Atmos. 125 (16). https://doi.org/10.1029/2019JD031668.

Kwok, R., 2018. Arctic sea ice thickness, volume, and multiyear ice coverage: losses and coupled variability (1958-2018). In: Environmental Research Letters, vol. 13, Issue 10. Institute of Physics Publishing. https://doi.org/10.1088/1748-9326/aae3ec.

Liu, Y., Key, J.R., Wang, X., Tschudi, M., 2020. Multidecadal Arctic sea ice thickness and volume derived from ice age. Cryosphere 14 (4), 1325–1345. https://doi.org/10.5194/tc-14-1325-2020.

Maffezzoli, N., Vallelonga, P., Edwards, R., Saiz-Lopez, A., Turetta, C., Kjær, H.A., Barbante, C., Vinther, B., Spolaor, A., 2019. A 120,000-year record of sea ice in the North Atlantic? Climate of the Past 15 (6), 2031–2051. https://doi.org/10.5194/cp-15-2031-2019.

Maffezzoli, N., Risebrobakken, B., Miles, M.W., Vallelonga, P., Berben, S.M.P., Scoto, F., Edwards, R., Kjær, H.A., Sadatzki, H., Saiz-Lopez, A., Turetta, C., Barbante, C., Vinther, B., Spolaor, A., 2021. Sea ice in the northern North Atlantic through the Holocene: evidence from ice cores and marine sediment records. Quat. Sci. Rev. 273. https://doi.org/10.1016/j.quascirev.2021.107249.

Maslanik, J., Stroeve, J., Fowler, C., Emery, W., 2011. Distribution and trends in Arctic sea ice age through spring 2011. Geophys. Res. Lett. https://doi.org/10.1029/2011GL047735.

Matoba, S., Niwano, M., Tanikawa, T., Iizuka, Y., Yamasaki, T., Kurosaki, Y., Aoki, T., Hashimoto, A., Hosaka, M., Sugiyama, S., 2018. Field activities at the SIGMA-A site, northwestern Greenland Ice Sheet, 2017. Bull. Glaciol. Res. 36, 15–22. https://doi.org/10.5331/bgr.18R01.

Meier, W.N., 2017. Losing Arctic sea ice: observations of the recent decline and the long-term context. In: Sea Ice, pp. 290–303. https://doi.org/10.1002/9781118778371.ch11.

Meier, W.N., Stewart, J.S., 2023. NSIDC Land, Ocean, Coast, Ice, and Sea Ice Region Masks. NSIDC Special Report 25. National Snow and Ice Data Center, Boulder CO, USA. https://nsidc.org/sites/default/files/documents/technical-reference/nsidc-special-report-25.pdf.

Meier, W., Fetterer, F., Savoie, M., Mallory, S., Duerr, R., Stroeve, J., 2013. NOAA/NSIDC Climate Data Record of Passive Microwave Sea Ice Concentration. Version 2. National Snow and Ice Data Center, Boulder, Colorado USA.

Meier, W.N., Perovich, D., Farrell, S., Haas, C., Hendricks, S., Petty, A.A., Webster, M., Divine, D., Gerland, S., Kaleschke, L., Ricker, R., Steer, A., Tschudi, M., Wood, K., 2021. Sea Ice, pp. 1–9.

Millero, F.J., Feistel, R., Wright, D.G., McDougall, T.J., 2008. The composition of Standard Seawater and the definition of the Reference-Composition Salinity Scale. Deep-Sea Research Part I: Oceanographic Research Papers. https://doi.org/10.1016/j.dsr.2007.10.001.

Mysak, L.A., Ingram, R.G., Wang, J., Van Der Baaren, A., 1996. The anomalous sea-ice extent in Hudson bay, Baffin bay and the Labrador Sea during three simultaneous NAO and ENSO episodes. Atmosphere - Ocean 34 (2), 313–343. https://doi.org/10.1080/07055900.1996.9649567.

Notz, D., SIMIP Community, 2020. Arctic sea ice in CMIP6. Geophys. Res. Lett. 47 (10), e2019GL086749. https://doi.org/10.1029/2019GL086749.

Osman, M., Das, S.B., Marchal, O., Evans, M.J., 2017. Methanesulfonic acid (MSA) migration in polar ice: data synthesis and theory. The Cryosphere 11 (6), 2439–2462. https://doi.org/10.5194/tc-11-2439-2017.

Osman, M., Das, S.B., Trusel, L.D., Evans, M.J., Fischer, H., Grieman, M.M., Kipfstuhl, S., McConnell, J.R., Saltzman, E.S., 2019. Industrial-era decline in subarctic Atlantic productivity. Nature 569 (7757), 551–555. https://doi.org/10.1038/s41586-019-1181-8.

Osman, M., Smith, B.E., Trusel, L.D., Das, S.B., McConnell, J.R., Chellman, N., Arienzo, M., Sodemann, H., 2021. Abrupt Common Era hydroclimate shifts drive west Greenland ice cap change. Nat. Geosci. 14 (10), 756–761. https://doi.org/10.1038/s41561-021-00818-w.

Rantanen, M., Karpechko, A.Y., Lipponen, A., Nordling, K., Hyvärinen, O., Ruosteenoja, K., Vihma, T., Laaksonen, A., 2022. The Arctic has warmed nearly four times faster than the globe since 1979. Communications Earth and Environment 3 (1), 1–10. https://doi.org/10.1038/s43247-022-00498-3.

Rigor, I.G., Wallace, J.M., Colony, R.L., 2002. Response of sea ice to the Arctic Oscillation. J. Climate 15 (18), 2648–2663. https://doi.org/10.1175/1520-0442(2002)015<2648:ROSITT>2.0.CO;2.

Sadatzki, H., Maffezzoli, N., Dokken, T.M., Simon, M.H., Berben, S.M.P., Fahl, K., Kjær, H.A., Spolaor, A., Stein, R., Vallelonga, P., Vinther, B.M., Jansen, E., 2020. Rapid reductions and millennial-scale variability in Nordic Seas sea ice cover during abrupt glacial climate changes. Proc. Natl. Acad. Sci. U. S. A. 117 (47), 29478–29486. https://doi.org/10.1073/pnas.2005849117.

Saiz-Lopez, A., Von Glasow, R., 2012. Reactive halogen chemistry in the troposphere. Chem. Soc. Rev. https://doi.org/10.1039/c2cs35208g.

Schmith, T., Hansen, C., 2003. Fram strait ice export during the nineteenth and twentieth centuries reconstructed from a multiyear sea ice index from southwestern Greenland. J. Climate 16 (16), 2782–2791. https://doi.org/10.1175/1520-0442(2003)016<2782:FSIEDT>2.0.CO;2.

Schweiger, A., Lindsay, R., Zhang, J., Steele, M., Stern, H., Kwok, R., 2011. Uncertainty in modeled Arctic sea ice volume. J. Geophys. Res. Oceans 116 (9). https://doi.org/10.1029/2011JC007084.

Scoto, F., Sadatzki, H., Maffezzoli, N., Barbante, C., Gagliardi, A., Varin, C., Vallelonga, P., Gkinis, V., Dahl-Jensen, D., Kjær, H.A., Burgay, F., Saiz-Lopez, A., Stein, R., Spolaor, A., 2022. Sea ice fluctuations in the Baffin Bay and the Labrador Sea during glacial abrupt climate changes. Proc. Natl. Acad. Sci. 119 (44), e2203468119. https://doi.org/10.1073/pnas.2203468119.

Semenov, V.A., Latif, M., 2012. The early twentieth century warming and winter Arctic sea ice. Cryosphere 6 (6), 1231–1237. https://doi.org/10.5194/tc-6-1231-2012.

Simpson, W.R., Carlson, D., Hönninger, G., Douglas, T.A., Sturm, M., Perovich, D., Platt, U., 2007. First-year sea-ice contact predicts bromine monoxide (BrO) levels at Barrow, Alaska better than potential frost flower contact. Atmospheric Chemistry and Physics. https://doi.org/10.5194/acp-7-621-2007.

Shumway, R.H., Stoffer, D.S., 2017. Time Series Analysis and Its Applications: With R Examples, Fourth Edition. Springer, ISBN 3319524526.

Simonsen, M.F., Baccolo, G., Blunier, T., Borunda, A., Delmonte, B., Frei, R., Goldstein, S., Grinsted, A., Kjær, H.A., Sowers, T., Svensson, A., Vinther, B., Vladimirova, D., Winckler, G., Winstrup, M., Vallelonga, P., 2019. East Greenland ice core dust record reveals timing of Greenland ice sheet advance and retreat. Nat. Commun. 10, 4494. https://doi.org/10.1038/s41467-019-12546-2.

Simpson, W.R., Brown, S.S., Saiz-Lopez, A., Thornton, J.A., Von Glasow, R., 2015. Tropospheric halogen chemistry: sources, cycling, and impacts. In: Chemical Reviews. https://doi.org/10.1021/cr5006638.

Smedsrud, L.H., Sirevaag, A., Kloster, K., Sorteberg, A., Sandven, S., 2011. Recent wind driven high sea ice area export in the Fram Strait contributes to Arctic sea ice decline. Cryosphere 5 (4), 821–829. https://doi.org/10.5194/tc-5-821-2011.

Smedsrud, L.H., Halvorsen, M.H., Stroeve, J.C., Zhang, R., Kloster, K., 2017. Fram Strait sea ice export variability and September Arctic sea ice extent over the last 80 years. Cryosphere 11 (1), 65–79. https://doi.org/10.5194/tc-11-65-2017.

Spolaor, A., Vallelonga, P., Plane, J.M.C., Kehrwald, N., Gabrieli, J., Varin, C., Turetta, C., Cozzi, G., Kumar, R., Boutron, C., Barbante, C., 2013. Halogen species record Antarctic sea ice extent over glacial-interglacial periods. Atmos. Chem. Phys. 13 (13), 6623–6635. https://doi.org/10.5194/acp-13-6623-2013.

Spolaor, A., Vallelonga, P., Gabrieli, J., Martma, T., Björkman, M.P., Isaksson, E., Cozzi, G., Turetta, C., Kjær, H.A., Curran, M.A.J., Moy, A.D., Schönhardt, A., Blechschmidt, A.M., Burrows, J.P., Plane, J.M.C., Barbante, C., 2014. Seasonality of halogen deposition in polar snow and ice. Atmos. Chem. Phys. https://doi.org/10.5194/acp-14-9613-2014.

Spolaor, A., Opel, T., McConnell, J.R., Maselli, O.J., Spreen, G., Varin, C., Kirchgeorg, T., Fritzsche, D., Saiz-Lopez, A., Vallelonga, P., 2016a. Halogen-based reconstruction of Russian Arctic sea ice area from the Akademii Nauk ice core (Severnaya Zemlya). Cryosphere 10 (1), 245–256. https://doi.org/10.5194/tc-10-245-2016.

Spolaor, A., Vallelonga, P., Turetta, C., Maffezzoli, N., Cozzi, G., Gabrieli, J., Barbante, C., Goto-Azuma, K., Saiz-Lopez, A., Cuevas, C.A., Dahl-Jensen, D., 2016b. Canadian arctic sea ice reconstructed from bromine in the Greenland NEEM ice core. Sci. Rep. 6. https://doi.org/10.1038/srep33925.

Spolaor, A., Barbaro, E., Cappelletti, D., Turetta, C., Mazzola, M., Giardi, F., Björkman, M.P., Lucchetta, F., Dallo, F., Aspmo Pfaffhuber, K., Angot, H., Dommergue, A., Maturilli, M., Saiz-Lopez, A., Barbante, C., Cairns, W.R.L., 2019. Diurnal cycle of iodine, bromine, and mercury concentrations in Svalbard surface snow. Atmospheric Chemistry and Physics 19 (20). https://doi.org/10.5194/acp-19-13325-2019.

Stein, A.F., Draxler, R.R., Rolph, G.D., Stunder, B.J.B., Cohen, M.D., Ngan, F., 2015. NOAA's HYSPLIT atmospheric transport and dispersion modeling system. Bull. Am. Meteorol. Soc. 96 (12), 2059–2077. https://doi.org/10.1175/BAMS-D-14-00110.1.

Stroeve, J., Holland, M.M., Meier, W., Scambos, T., Serreze, M., 2007. Arctic sea ice decline: faster than forecast. Geophys. Res. Lett. 34 (9), L09501. https://doi.org/10.1029/2007GL029703.

Strong, C., Magnusdottir, G., 2010. Modeled winter sea ice variability and the North Atlantic Oscillation: a multi-century perspective. Climate Dynam. 34 (4). https://doi.org/10.1007/s00382-009-0550-7.

Tang, C.C.L., Ross, C.K., Yao, T., Petrie, B., DeTracey, B.M., Dunlap, E., 2004. The circulation, water masses and sea-ice of Baffin Bay. In: Progress in Oceanography, vol. 63, Issue 4. https://doi.org/10.1016/j.pocean.2004.09.005.

Thomas, E.R., Allen, C.S., Etourneau, J., King, A.C.F., Severi, M., Winton, V.H.L., Mueller, J., Crosta, X., Peck, V.L., 2019. Antarctic sea ice proxies from marine and ice core archives suitable for reconstructing sea ice over the past 2000 years. Geosciences (Switzerland) 9 (12). https://doi.org/10.3390/geosciences9120506.

Trenberth, K.E., Shea, D.J., 2006. Atlantic hurricanes and natural variability in 2005. Geophys. Res. Lett. 33, L12704. https://doi.org/10.1029/2006GL026894.

Tschudi, M., Meier, W.N., Stewart, J.S., Fowler, C., Maslanik, J., 2019. EASE-Grid Sea Ice Age, Version 4 [Data Set]. Snow and Ice Data Center Distributed Active Archive Center. NASA National Snow and Ice Data Center Distributed Active Archive Center, Boulder, Colorado USA. https://doi.org/10.5067/UTAV7490FEPB. Date Accessed 05-18-2024.

Vallelonga, P., Maffezzoli, N., Moy, A.D., Curran, M.A.J., Vance, T.R., Edwards, R., Hughes, G., Barker, E., Spreen, G., Saiz-Lopez, A., Corella, J.P., Cuevas, C.A., Spolaor, A., 2017. Sea-ice-related halogen enrichment at Law Dome, coastal East Antarctica. Clim. Past 13 (2), 171–184. https://doi.org/10.5194/cp-13-171-2017.

Vallelonga, P., Maffezzoli, N., Saiz-Lopez, A., Scoto, F., Kjær, H.A., Spolaor, A., 2021. Sea-ice reconstructions from bromine and iodine in ice cores. In: Quaternary Science Reviews, vol. 269. https://doi.org/10.1016/j.quascirev.2021.107133.

Walsh, J.E., Fetterer, F., Scott Stewart, J., Chapman, W.L., 2017. A database for depicting Arctic sea ice variations back to 1850. Geogr. Rev. 107 (1). https://doi.org/10.1111/j.1931-0846.2016.12195.x.

Walsh, J.E., Chapman, W.L., Fetterer, F., Stewart, J.S., 2019. Gridded Monthly Sea Ice Extent and Concentration, 1850 Onward, Version 2. National Snow and Ice Data Center, Boulder, Colorado USA. https://doi.org/10.7265/jj4s-tq79 (Date Accessed 05-09-2024).

Wei, J., Zhang, X., Wang, Z., 2019. Reexamination of Fram Strait sea ice export and its role in recently accelerated Arctic sea ice retreat. Climate Dynam. 53 (3–4), 1823–1841. https://doi.org/10.1007/s00382-019-04741-0.

Yang, Y., Min, C., Luo, H., Kauker, F., Ricker, R., Yang, Q., 2023. The evolution of the Fram Strait sea ice volume export decomposed by age: estimating with parameter-optimized sea ice-ocean model outputs. Environ. Res. Lett. 18 (1). https://doi.org/10.1088/1748-9326/acaf3b.